



Investigation on machinability of NiTi shape memory alloys under different cooling conditions

Yanzhe Zhao^{1,2} · Kai Guo^{1,2} · Jianfeng Li^{1,2} · Jie Sun^{1,2}

Received: 3 December 2020 / Accepted: 27 June 2021 / Published online: 5 July 2021
© The Author(s), under exclusive licence to Springer-Verlag London Ltd., part of Springer Nature 2021

Abstract

NiTi shape memory alloy products are becoming more and more popular in many areas. But owing to the unique characteristics of NiTi shape memory alloys, it is still considered restrictive by the traditional machining methods of producing NiTi shape memory alloys for finished products. Flood coolant and cryogenic with liquid nitrogen (LN₂)–assisted machining is desired to improve machinability of material in the turning procedure. Experiments were conducted to examine the influence of cooling conditions (dry, flood, and cryogenic LN₂) on turning NiTi shape memory alloys at different cutting speeds. Tool wear, cutting force, and surface integrity were selected as evaluation characteristics to explore the effects of different cooling methods and the stress-induced martensitic phase during the turning process. The study shows that the appearance of the stress-induced martensitic phase during the turning process harms the machinability of NiTi shape memory alloys. Flood conditions accomplish lower tool wear and cutting force at 15 m/min. Cryogenic conditions achieve higher machinability at 125 m/min.

Keywords NiTi shape memory alloys · Stress-induced martensitic phase · Cutting condition · Phase

1 Introduction

NiTi shape memory alloy is an innovative material, which has great application potential [1]. Because of its shape memory effect, superelasticity, corrosion resistance, excellent fatigue properties, and high resistance [2], it has been widely accepted as a smart material in the aerospace industry, medicine, construction industry, and robotics [3]. However, the favorable properties also bring challenges while machining it. Other properties of NiTi shape memory alloys, like high specific heat, low thermal conductivity, and Young's modulus, make it difficult to machine [4, 5]. High temperature, tool wear,

strain hardening, and poor surface quality are the problems for machining this unique shape memory alloy. In the machining process, cutting fluid can effectively reduce cutting temperature and friction coefficient between the tool and workpiece. It is an essential component that affects the sustainability of the overall process [6]. Meanwhile, it is well-known that cryogenic coolants also improve the machining performance when machining the difficult-to-cut alloys [7]. It can decrease the cutting temperature effectively and increase the tool life [8]. Therefore, taking advantage of the cutting fluid and cryogenic coolant may improve the machinability of NiTi shape memory alloy. The cutting characteristics under different cutting conditions should be analyzed to understand the cutting mechanisms. Meanwhile, the exploration of a proper method for turning NiTi shape memory alloy is necessary to improve the machinability and reduce the production cost of NiTi alloy products.

With the accretion of demand and technique progress, researchers are getting more attention on the conventional machining NiTi shape memory alloy. At first, researchers were devoted to the NiTi shape memory alloy's machinability after a series of cutting experiments. The strain hardening during the cutting process caused an extensive hardened layer on the machined surface, and the NiTi shape memory alloy exhibited more difficult cutting characteristics than other metal alloys

✉ Kai Guo
kaiguo@email.sdu.edu.cn

✉ Jie Sun
sunjie@sdu.edu.cn

¹ Key Laboratory of High-efficiency and Clean Mechanical Manufacture, National Demonstration Center for Experimental Mechanical Engineering Education, School of Mechanical Engineering, Shandong University, Ji'nan 250061, Shandong, China

² Research Center for Aeronautical Component Manufacturing Technology & Equipment, Shandong University, Ji'nan 250061, Shandong, China

[9]. The high strain-rate hardening, unique pseudoelasticity, and high toughness of this material were the main reasons for the processing performance of NiTi SMAs, which were presented by Lin et al. [4]. Biermann et al. [10] compared the machinability between martensitic and austenitic NiTi alloys during the micro-milling process. Guo et al. [11] presented that the high strength and specific heat were the main reasons for tool wear, and an austenitic white layer occurred on the surface of milling. Subsequently, experiments of searching for the best cutting parameters were carried out. Weinert et al. [12] used different inserts during turning NiTi alloys process suggesting that a cutting speed of 100 m/min and depth of cut less than the corner radius accomplished less tool wear. Kuppuswamy et al. [13] optimized the cutting parameters as a focused study on reducing the micro-milling forces and the formation of burr; the lowest cutting force and burr size are achieved at 15 m/min. Biermann et al. [14] analyzed the quality of the drilled holes at different cutting parameters and concluded that the cutting speed should not exceed 30 m/min to decrease the work hardening. The optimum feed is 5 μm when the diameter of the tool is 1 mm. Wang et al. [15] carried out an orthogonal experiment of milling NiTi SMA to study the work hardening of the machined sample. The cutting speed affects the work hardening mostly, which affects the machining-induced layer's depth. Moreover, some researchers also analyzed the influence of different cutting conditions on the processing of NiTi SMAs. Weinert et al. [16] concluded that the cooling lubricant has a positive effect on the poor chip breaking and tool life during the turning process. However, the poor chip breaking cannot be solved by it. Yusuf et al. [17] compared different machining conditions on machining NiTi alloys and concluded that cryogenic machining improves the machinability of NiTi alloys. Zailani et al. [18] applied chilled air to the micro-milling of NiTi shape memory alloys; lower burr height, and cutting forces are achieved. Rosnan et al. [19] conducted drilling experiments on NiTi alloys under flood and minimal quantity lubricants reinforced with nano-particles (MQLn) conditions and concluded that MQLn significantly decreases the thrust force and negatively affects the surface quality.

It is clear from the literature reviews that many methods were used to explore a better way of machining the NiTi shape memory alloys. However, the specific reasons for improving the NiTi shape memory alloy's machinability were not discussed in detail. In the study, three different cutting conditions, dry, flood with mineral oil-based cutting fluids (flood), and cryogenic with liquid nitrogen (LN_2), are applied in turning NiTi shape memory alloys at different cutting speeds for comparative analysis. Cutting force, cutting temperature, tool wear, phase transformation, and surface integrity are investigated in this research work.

The effects of the stress-induced martensitic phase during the turning process on tool wear, cutting force, and surface

roughness are first investigated in this work. It attributes to interesting results which are different from that of other metal material. The effect of machining on the phase state is analyzed to observe the NiTi shape memory alloy's functional behaviors. Meanwhile, different cutting conditions on the workpiece causes different machining effects at numerous cutting speeds. Different processing performances of the martensite and austenite phases are discussed in this paper. It provides the basis for the NiTi shape memory alloy's machinability.

2 Experiment

2.1 Work materials

A Ni55.8Ti44.2 (wt%) shape memory alloy of 300 mm length and 20 mm diameter is used in this experiment. Seven tests were performed at seven different cutting speeds under three cutting conditions. The phase transformation of machined and as-received specimens was analyzed by the X-ray diffraction (XRD) patterns. An Ultima IV was used to get the XRD patterns at a scan speed of $10^\circ/\text{min}$ within the range of 20 to 80 degrees and plot 2θ (degree) XRD scans at 25°C . The XRD patterns of as-received specimens are showed in Fig. 1; the austenite (B2) diffraction peak with (110), (200), and (211) Miller indexes are shown. The four-phase inversion temperature was obtained from the differential scanning calorimetry (DSC) curve, measured by using the Netzsch DSC3500 Sirius. The start temperature of martensite transformation M_s is -35°C , the finish temperature of martensite transformation M_f is -53°C , the start temperature of the reverse of austenite transformation A_s is -13°C , and the finish temperature of the reversal of austenite transformation A_f is -2°C . The material's emissivity was 0.21.

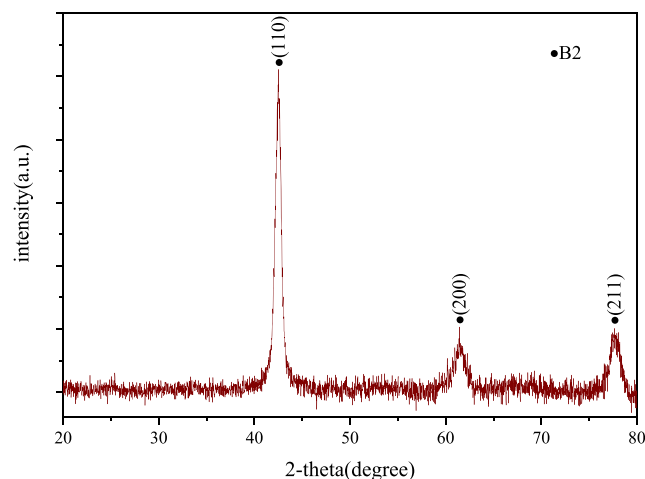


Fig. 1 The XRD patterns of as-received specimens

2.2 Experimental procedure

The cutting insert was a PVD-coated carbide insert (VNMG160408-SM1105) with TiAlN coating, which was chosen due to the minimum wear observed in previous experimentation [20]. The cutting experiment was conducted on a C6140H turning machine with a maximum revolution of 1980 revolutions per minute (RPM). At each cutting conditions (dry, flood, LN₂), the workpiece machined at varied cutting speeds (v_c), 7.5, 15, 22, 33, 47, 87, and 125 m/min, with the feed rate of 0.15 mm/r and depth of cut is 0.2 mm. Twenty millimeters is the cutting length for each test. To eliminate the tool wear's effect, the insert was replaced by a new one after a single test. A handheld microscope (Dino Capture 2.0) was used to obtain the tool wear. The cutting force was measured by using the Kistler 9257B dynamometer, and the FORTIC 226 infrared radiation imaging sensor was used to collect the cutting temperature. The experimental details are summarized in Table 1.

The average surface roughness (Ra) was obtained by using a TR200 mobile surface roughness meter. The optical microscope KEYENCE VHX-600 is used to observe the surface morphology. The cutting fluids and liquid nitrogen are applied by different sprays, which are approached to the tool-workpiece contact area. The experimental setup is

Table 1 Experimental details

Items	Descriptions
Workpiece	
Material	Nickel-titanium shape memory alloy
Dimensions	Φ 20 mm × 250 mm
Lathe	C6140H (n_{\max} = 1980 r/min)
Cutting tool	
Material	PVD-coated carbide insert, Sandvick
Coating	TiAlN
Cutting parameters	
Cutting speed (v_c)	7.5 m/min, 15 m/min, 22 m/min, 33 m/min, 47 m/min, 87 m/min, 125 m/min
Feed rate (f)	0.15 mm/r
Depth of cut (a_p)	0.2 mm
Cutting conditions	Dry, flood, LN ₂
Measurement	
Cutting force	Kistler 9257B dynamometer
Cutting temperature	FORTIC 226 infrared radiation imaging sensor
Tool wear	Dino Capture 2.0
Surface morphology	KEYENCE VHX-600
Average surface roughness	TR200 mobile surface roughness meter

showed in Fig. 2. And the flow chart of the experiment is depicted in Fig. 3.

The cryogenic cooling equipment used in this experiment consists of a cryogenic dewar tank (50 L), a self-pressurized liquid nitrogen pump, and a nozzle made of copper. The compressor generates negative pressure to absorb liquid nitrogen into the vaporizing chamber. Because liquid nitrogen vaporizes quickly when the pressure drops, some liquid has to vaporize and expand into the vaporizing chamber. After that, the increased pressure yields the liquid nitrogen (LN₂), which has not yet evaporated to the nozzle via the pipe encased with an insulating material. The liquid nitrogen gets sprayed to the interface between the tool and the workpiece via a nozzle at 0.3 bar of pressure, as shown in Fig. 4.

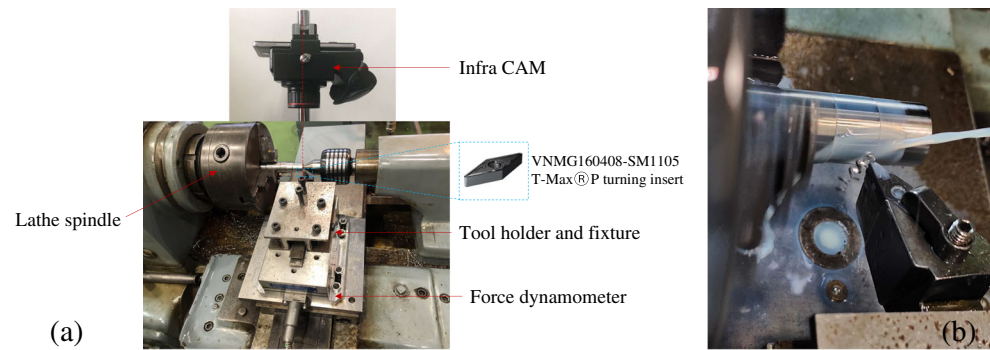
3 Results and discussion

3.1 Tool wear

The inserts that have been machined are collected, and the wear morphology is magnified 200 times through the Dino Capture 2.0. Wear morphology on the rake and flank face at 15 m/min and 125 m/min under dry, flood, and LN₂ conditions is shown in Fig. 5. Tool wear is less under these experimental parameters, and all coating on the rake surface is found to be worn off. Because of the high ductility of NiTi alloy, the abrasion wear can be obtained on the rake and flank face [5, 21]. Grooves along chip flow direction can be easily seen at 15 m/min under three conditions, which indicate the abrasion wear mechanism [8]. At 15 m/min, the rake surface's coating is worn off on account of the chip flow on the tool face. The multiple deep scratches can be seen on the flank face of the insert [22]. Furthermore, because of the high strain hardening of NiTi shape memory alloy, it can be seen with the built-up edge (BUE) on the flank face. At 125 m/min, the cutting temperature gets concentrated at the tool edge and the chips on account of the low thermal conductivity and high specific heat. The chip formation flows on the surface, leading to higher temperature and pressure on the contact area between tool and chip, and crater wears starts to occur on the rake face. Meanwhile, the adhesion wear can be observed under dry and flood conditions because of the high cutting temperature. An interesting result is that the tool wear is minimal at 125 m/min under cryogenic conditions. Cryogenic conditions play a prominent positive role in decreasing the tool wear because of the lower temperature in the tool-chip area [23].

According to the ISO 3685 standards (average flank wear, $VB \geq 0.3$ mm), the flank wear is measured three times and takes the average. The average flank wear under different cutting conditions are shown in Fig. 6. For flood conditions, it offers a remarkable effect on reducing the flank wear when

Fig. 2 Schematic of an experimental setup; (a) dry machining and (b) flood machining



the cutting speed is below 33 m/min. Because there are tiny clearance exits between the chip and rake of the tool, the capillary phenomena are occurred. Mineral oil-based cutting fluids flow into the cutting area at the lower cutting speed; a lubricating film is formed. The extent of direct contact between metals decreases, which decreases the friction coefficient in the contact area.

Meanwhile, cutting fluid flow takes away a lot of produced cutting heat and reduces the cutting temperature. The effect of lubrication and cooling reduces the flank wear. However, as the cutting speed increases, there is an inadequate supply of cutting fluid between the workpiece and tool, and the lubrication effect is negligible. For cryogenic conditions, it reduces the flank wear significantly compared with dry machining. Mostly, it performs suitably when the cutting speed above 33 m/min. A lower cutting temperature greatly affects the flank wear. However, when the cutting speed is below 33 m/min, the wear extent is a little greater than that of the flood conditions, which will be discussed later.

3.2 Cutting force

The cutting forces during machining of the samples are collected, and the mean values of different cutting forces at different speeds are shown in Figs. 7, 8, and 9. The main cutting force, radial force, and feed force are presented, respectively. The main cutting force is slightly higher than the radial force, and the feed forces are about 30% of the main cutting force. This value is almost the same as Inconel 718 [24], and the geometry of the cutting tool leading to this result [25].

The results indicate that cutting speed influence the cutting force slightly. Some reports in the early literature show that the cutting force changes insignificantly at varying cutting speeds. In contrast, the feed rate and depth of cut affect the cutting force greatly [25, 26]. This is because the cutting force is more sensitive to geometrical factors than cutting speed conditions [27]. From the overall trend, when the cutting speed is below 33 m/min, the cutting force initially decreases and then increases. The high ductility of the material, which is easy to weld on the cutting tool, results in the BUE. The formation and disappearance of the BUE, which influences the tool rake angle, result in the cutting force. At a higher cutting speed (higher 33 m/min), the cutting force continues to decrease. At the same time, the friction coefficient reduced with the increasing cutting speed. Finally, as the cutting temperature increases by leading to a better thermal softening, work hardening is further reduced.

However, the cutting conditions have different influences on the cutting force. For flood conditions, at a lower cutting speed (33 m/min), the lubrication has a positive effect on cutting forces. The friction between workpiece and tool reduced, and the cutting force decreased to a certain extent. Nevertheless, as the cutting speed increases, the lubrication effect is negligible, and the cutting force is very similar to that of the dry conditions. For cryogenic with LN₂, interesting results have occurred; the cooling conditions do not reduce the cutting force than dry conditions. This result is different from the previous study observed in shape memory alloys [28].

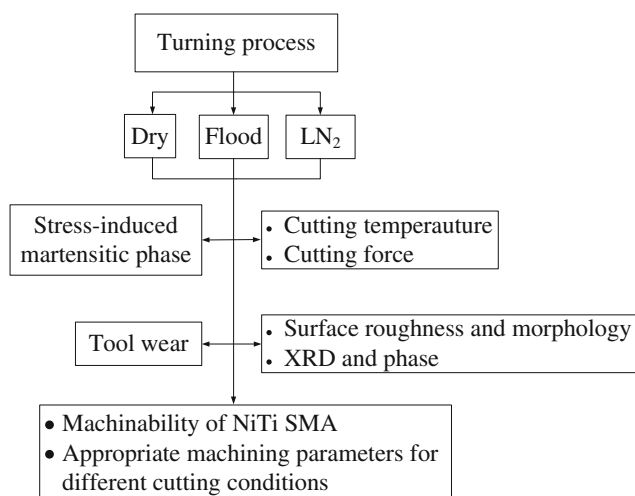
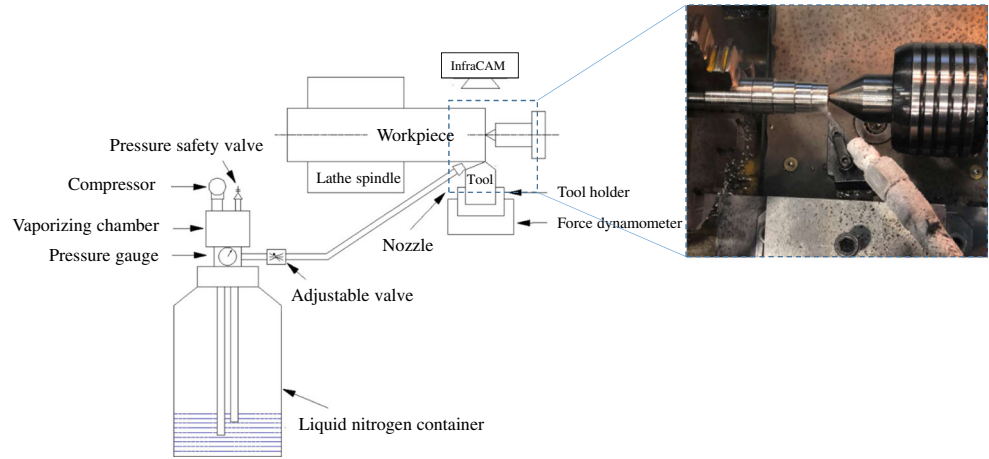


Fig. 3 Flow chart of experiment

Fig. 4 Schematic of cryogenic cooling equipment



On the one hand, in Kaynak’s work, the workpiece was pre-cooled and machined using liquid nitrogen. It is a fully martensitic state or partially martensitic state before and under machining by pre-cooling and using liquid nitrogen during machining, while it is in an austenitic state before and under dry conditions. The workpiece in the martensitic state is softer than that in the austenitic state. So the cutting force is lower than that of the dry condition in that experiment, while, for the workpiece used in this experiment, the liquid nitrogen is used for cooling only during the process. The austenitic state does not change as the cutting temperature goes up. So the workpiece is in an austenitic state before and under machining.

On the other hand, in Kaynak’s experiment, a couple of nozzles were placed at the flank face and the rake face, the temperature was well-controlled, and the cutting tool’s hardness increased, which decreased cutting force. Indeed, the nozzle used in this experiment is only focused on the tool-chip connect area. During machining, the low temperature caused by the LN₂ cutting fluids caused an increase in the workpiece’s flow stress, which caused a higher cutting force in cryogenic conditions [29].

For the main cutting force component, when the cutting speed is below 33 m/min, the main force is the lowest at 15 m/min. The flood conditions reduce the main force effectively. A lubricating film is established at this cutting speed. At a

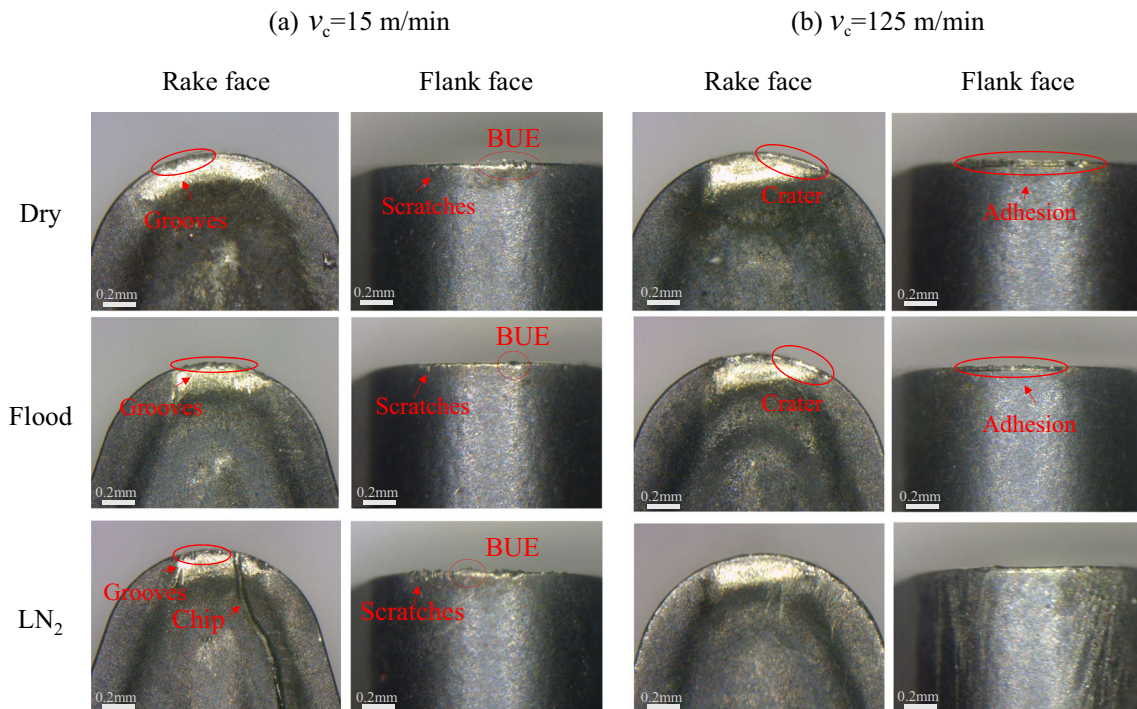


Fig. 5 The wear morphology of the insert at different conditions after machining

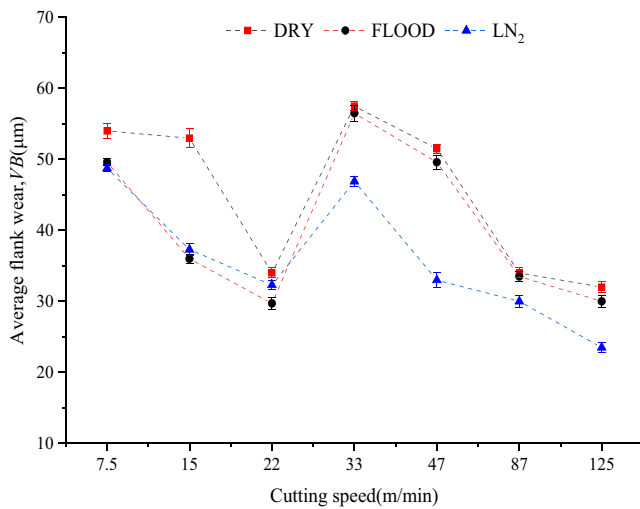


Fig. 6 The average flank wear under dry, flood, and LN₂ cutting conditions

higher cutting speed (higher 33 m/min), the coolant becomes challenging to throw into the interface of the tool-workpiece area. The lubrication and cooling effect are minimal. Figure 8 shows the radial force recorded under different conditions at various cutting speeds. There is little difference between the three conditions. At 15 m/min and 125 m/min, it showed a lower radial force. Figure 9 shows the trend of feed force with the increasing cutting speeds in various conditions. The fluctuation of the feed force is relatively larger than the other two forces, which causes plowing on the machined surface. When the cutting speed is lower than 33 m/min, the fluctuation of feed force is larger in flood and cryogenic conditions than that in dry conditions, and the flow of the lubricants and LN₂ has more influence on it. As the cutting speed increases, its impact is getting smaller.

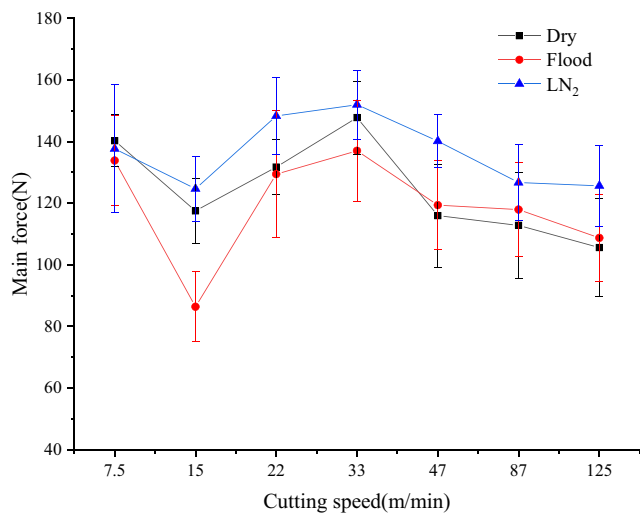


Fig. 7 The main cutting force under different cutting speeds and cutting conditions

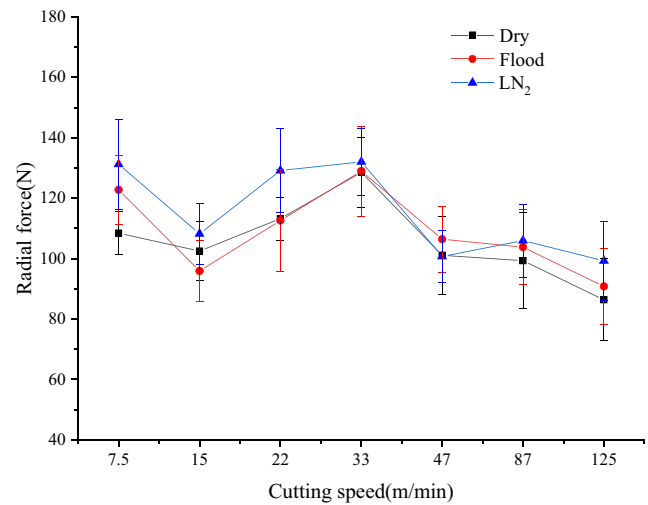


Fig. 8 Radial force under different cutting speeds and cutting conditions

3.3 Cutting temperature

In the cutting process, extremely high strains and plastic deformation occur in the material; the energy required to deform is released in heat. The generated heat at the tool-workpiece contact area is essential to the cutting performance. Generally, most of the generated heat is dissipated to the chip and tool for metal machining. The highest temperature occurred at the tool-workpiece contact area. So, the temperature at the tool-workpiece contact area is recorded by using the infrared radiation imaging sensor, as showed in Fig. 10. The average cutting temperature under steady cutting conditions is taken for analysis.

Figure 11 shows the cutting temperature in different conditions and cutting speeds. As the cutting speed increases, the cutting temperature increases during other cutting process conditions. Firstly, with the rise of cutting speed, the cutting process becomes more adiabatic, and the generated heat cannot rapidly dissipate in a short time. Secondly, as cutting speed

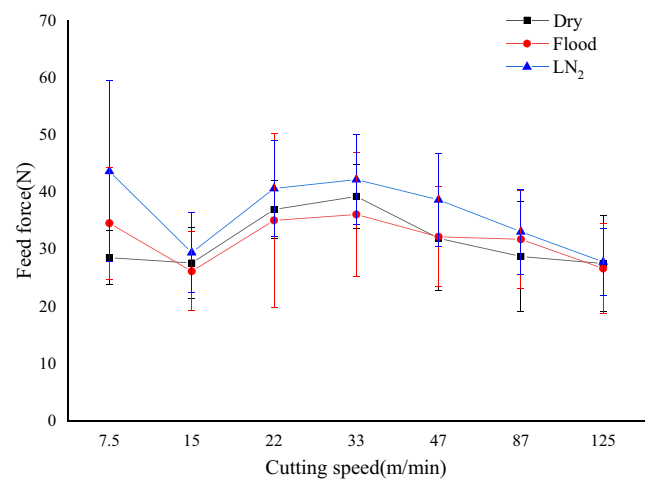


Fig. 9 Feed force under different cutting speeds and cutting conditions

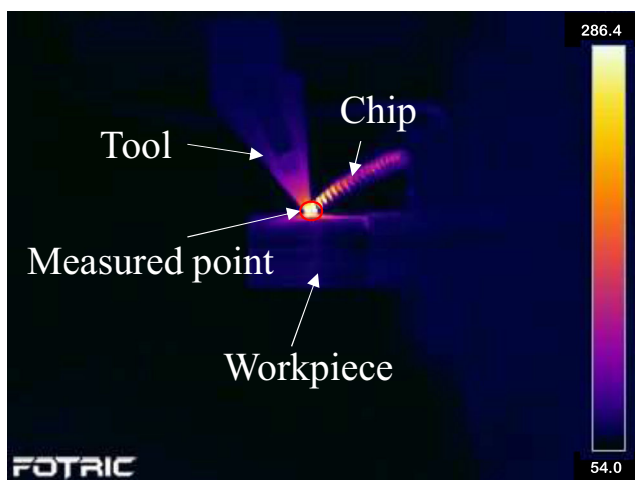


Fig. 10 The measured point during the process

increases, less and less cutting fluid enters the cutting area; the effect of cooling and lubrication decreases at higher cutting speeds. Compared with dry machining, flood and cryogenic conditions have obvious effectiveness in reducing the cutting temperature. The lower cutting temperature increases the tool's hardness and results in a better performance in machinability [30]. Moreover, the cutting temperature decreases even more under cryogenic conditions.

For dry conditions, the cutting temperature is in the range of 419–582 °C. At the same time, it is 183–396 °C in flood conditions and 96–346 °C in cryogenic conditions. For NiTi shape memory alloy, there is martensite desist temperature (M_d). When the temperature is between A_f temperature and M_d temperature, the critical stress of stress-induced martensite transformation (σ_{ms}) is less than the austenitic dislocation slip critical stress (σ_A); there is stress-induced martensite occurring during the loading and unloading process. If the temperature is higher than M_d temperature, the $\sigma_{ms} > \sigma_A$, there is just austenite phase deformation existing in the workpiece during

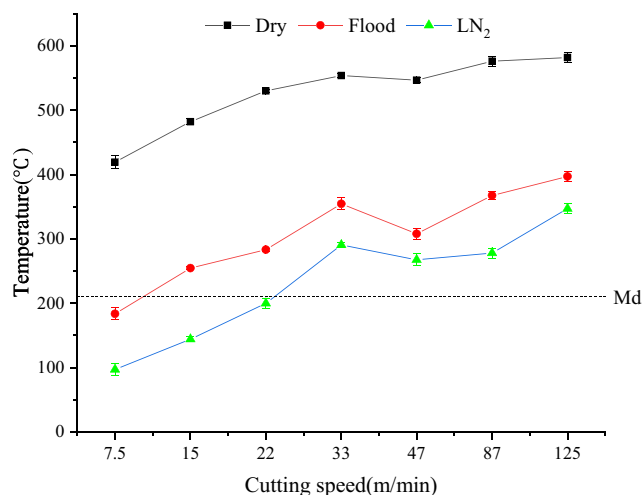


Fig. 11 Cutting temperature at varied cutting speeds in different conditions

the loading and unloading process. From a crystal point of view, the crystal structure of the austenitic phase is a high-symmetry body-centered cubic. In contrast, the stress-induced martensitic phase is an asymmetry cubic structure [31]. The austenitic phase is tightly packed and hard, while the martensitic phase has higher ductility and softening.

Meanwhile, it is essential to note that the ductility of the austenitic phase is still recorded high [32]. For the near-equal atomic ratio NiTi shape memory alloy, Benafan et al. [32] presented that the M_d temperature was between 310 and 330 °C by performing the loading and unloading experiment at various temperatures. Moreover, the M_d temperature was associated with the M_s . For the workpiece used in this experiment, the M_d temperature is about 210 °C. So there is no stress-induced martensitic phase that occurred during dry machining. During flood conditions, at 10 m/min, the stress-induced martensitic phase appears due to the tensile deformation. Just the austenite phase exists when the cutting speed is above 15 m/min. For cryogenic conditions, more than 25 m/min, the cutting temperature is higher than the M_d temperature; no stress-induced martensitic phase appeared during the cutting process. Therefore, the stress-induced martensitic phase should be noticeable during the experiment, and it will be discussed later.

3.4 The influence of stress-induced martensitic phase

In combination with the tool wear, when the cutting speed is less than 33 m/min, though the cutting temperature is about 100 °C higher in flood conditions than in cryogenic conditions, the flank wear is a little server in the cryogenic condition than that in flood conditions. Moreover, the chip is easy to stick to the rake surface. This condition is observed because the stress-induced martensitic phase generated in cryogenic conditions. The martensitic phase is soft, which is easy to stick on the insert. When the cutting speed is above 33 m/min, the cutting temperature gets increased. Only the austenite phase is observed during machining in these three conditions; the cryogenic conditions perform a remarkable effect on the flank wear due to reducing the cutting temperature. So the stress-induced martensitic phase promotes the tool wear.

Combined with the changes of cutting force, it is only in the austenite phase during machining under the three conditions when the cutting speed is above 33 m/min. And the cutting force reduces with the increase of cutting temperature. This condition happens owing to the yield stress, which decreases with the increased temperature, and the thermal softening gets increased with the increased cutting temperature. From Fig. 7, the cutting force under dry condition is less than that of the under flood and cryogenic conditions because of a higher thermal softening effect caused by a higher cutting temperature. So the cutting temperature affects the cutting force greatly at higher cutting speeds.

When the cutting speed is less than 33 m/min, there is a stress-induced martensitic phase generated in cryogenic conditions, while there is only the austenite phase in dry conditions. Generally, the martensitic phase is softer than the austenite phase. However, from the results in Fig. 7, the main cutting force in the cryogenic condition is higher than that in dry conditions. Meanwhile, at 7.5 m/min, the stress-induced martensitic phase occurred in flood and cryogenic conditions. However, the cutting temperature differs by nearly 100 °C; the main cutting force difference between the three conditions is less than 10 N, and the cutting temperature affects the cutting force slightly. A conclusion can be made that though the softened martensitic phase occurred during the cutting process, it has little influence on the cutting force. Consequently, the built-up edge is the key influencing factor for the cutting force at lower cutting speeds.

3.5 Surface roughness and morphology

The surface roughness is the most intuitive indicator of surface quality; it is related to the functional characteristics of the surface and the performance of the parts. As explained above, the state of NiTi samples is different in different cutting speeds under various cutting conditions. The average surface roughness (R_a) at typical cutting speeds under these three cutting conditions is shown in Fig. 12.

Surface roughness decreases as the cutting speed increases, indicating that a higher cutting speed achieves a better surface roughness for machining NiTi shape memory alloy. This indication is mainly because of the top of the BUE repeatedly growing and dividing at lower cutting speed, causing the fluctuation of cutting force [33], and increasing the surface roughness. The BUE disappears with the increased cutting speed, and the effect of thermal softening exceeds that of work hardening high speed [34, 35]. Hence, a smoother surface is achieved at high speed. Meanwhile, the flood condition performs better result in reducing the R_a . However, it is surprising that the surface roughness produced under the LN_2 condition is bigger than dry and flood turning. This is attributed to the appearance of the stress-induced martensitic phase.

At 7.5 m/min, the NiTi sample is a martensitic phase during turning under flood and LN_2 conditions and is in the austenite phase under dry conditions. On the one hand, the soft martensitic phase sticks on the tool, making it easier to form BUE. On the other hand, because of the high ductility of NiTi shape memory alloy, parts of the material are pushed out of the contact zone. Then, instead of cutting away, the burrs form on the machined surface [16]. In flood conditions, the coolant is well-accessed inside the tool-workpiece contact area at the lowest cutting speed, providing a better lubrication performance.

Moreover, the cutting temperature is close to the M_d temperature, and the martensite phase's volume fraction is smaller

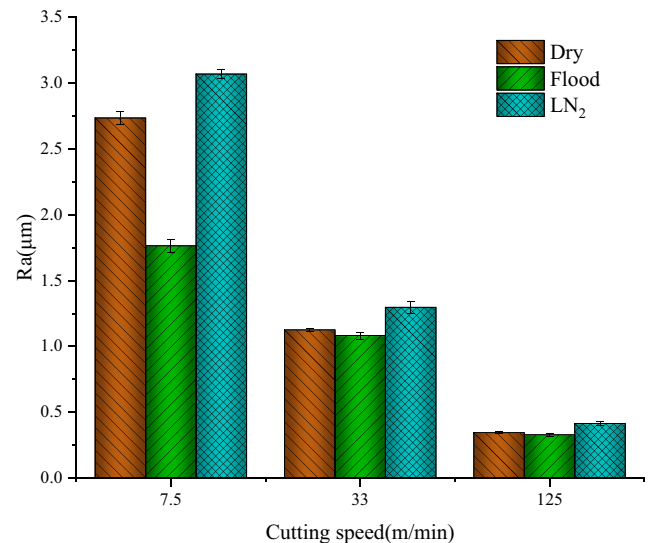


Fig. 12 The average surface roughness at typical cutting speeds under different cutting conditions

than those in the LN_2 condition. At the same time, the lowest surface is achieved in a flood condition at 7.5 m/min. It can be inferred that lubrication plays a vital role in surface roughness when machining NiTi shape memory alloy at this speed. At 33 m/min, it is the austenite phase in dry and flood conditions. While in LN_2 condition, part of the material undergoes a stress-induced martensitic transformation, causing R_a value to be 15% higher than that of dry condition. At 125 m/min, it is in austenite phase in three conditions. The surface roughness is almost the same in three conditions which are less than 0.5 μm , which reaches a good surface finish.

The optical images of machined surface morphology at typical cutting speeds, under dry, flood, and LN_2 cutting conditions are shown in Fig. 13. The surface morphology matches well with the surface roughness. There are many defects on the machined surface at 7.5 m/min, which result in high surface roughness; a smoother surface obtained at 125 m/min, and low surface roughness is accomplished.

There are feed marks and metal debris on the machined surface at low speed. It is mainly because of the formation of BUE. On the one hand, the irregular shape of BUE is causing the inconsistent overcut at each point on the insert. Grooves of different depth and width along the direction of cutting speed are also depicted. On the other hand, the detached BUE from the tool gets transferred to the machined surface and stick on it, causing the metal debris [36]. Though the surface is smooth at high cutting speed, there are long grooves that exist on it. Since the average flank wear (VB) is less than 0.1 mm from Fig. 6, the tool is in the early stage of breakage. The sharper cutting edge reduces the contact area and increases the pressure stress, leading to the long and light grooves.

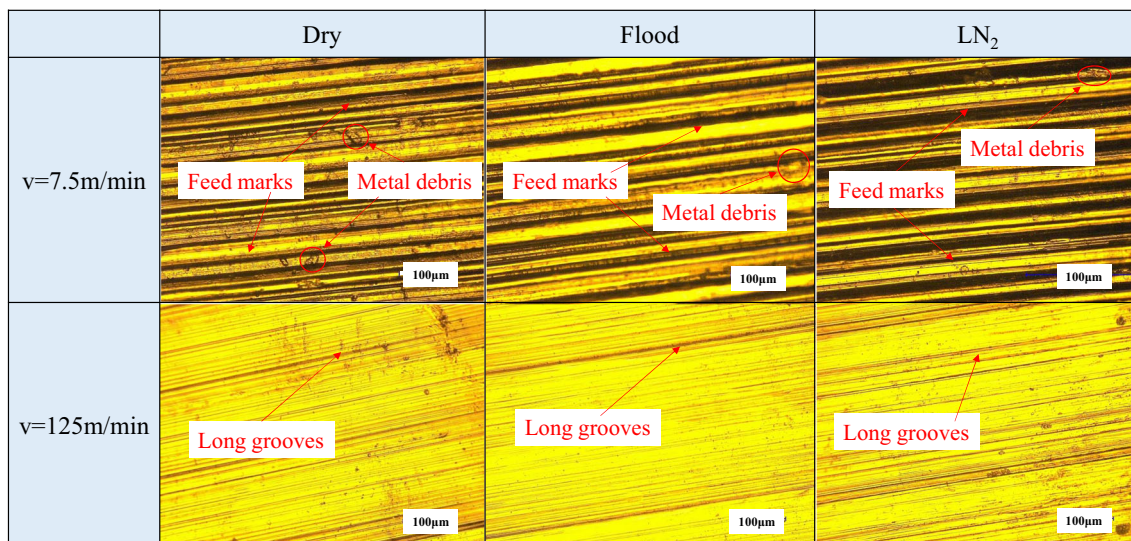


Fig. 13 Surface morphology of machined surface at typical cutting speeds under the different cutting conditions

3.6 XRD and phase

NiTi shape memory alloy is sensitive to temperature and stress because of its unique property. There is high stress, high strain, and high temperature during the turning process, which will influence the phase state of the material on the surface and subsurface. Therefore, the phase state on the machined surface should be observed to achieve the desired functional behaviors. The XRD patterns of the machined surface at two typical cutting speeds (15, 125 m/min) are shown in Figs. 14 and 15.

At a lower cutting speed, under dry and flood conditions, the B2 diffraction peak with the Miller index is the same as the as-received one. In contrast, only diffraction peak with (110) and (211) Miller index exists in cryogenic conditions. Furthermore, the diffraction peak broadened after machining under dry and flood conditions, and the height of the

diffraction peak is increased under dry and flood conditions while decreased under LN₂ conditions. Though there is a stress-induced martensitic phase during machining at this cutting speed, completely martensite reverse transformation occurred after machining. The broadened peak indicates that the residual stress exists in the material, and the stress is less than the σ_{ms} value because there is no martensitic phase shown in the XRD patterns. So at a lower cutting speed, the generated residual stresses in the machined samples have little influence on the phase state in the machined samples.

Meanwhile, the dislocation density and defects increased by the stress effect [23]. The higher peak indicates that the microstructure is more uniform after the mechanical effect. Consequently, under flood conditions, a more uniform microstructure is displayed. Under the cryogenic conditions, though there is less residual stress on the surface, the microstructure

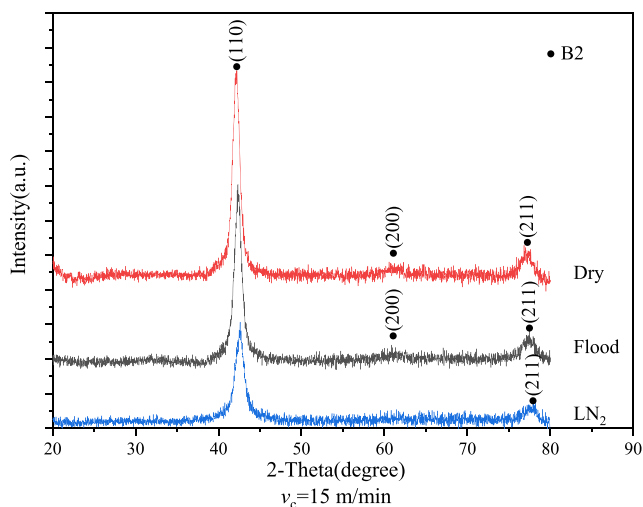


Fig. 14 XRD patterns of the machined surface at 15 m/min under different conditions

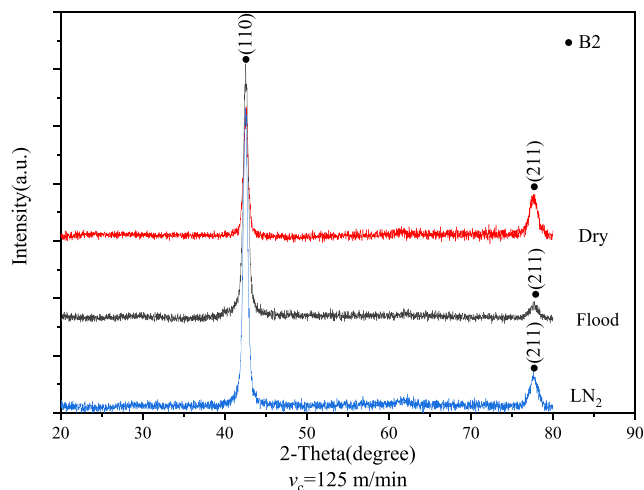


Fig. 15 XRD patterns of the machined surface at 125 m/min under different conditions

may be less consistent than that in an as-received one. This result is because of the tool wear and the fluctuation of cutting force at this cutting speed under cryogenic conditions.

The diffraction peak broadened a little under three conditions at a higher cutting speed, and the relative intensity is increased, especially in flood and cryogenic conditions. Residual stresses on the machined surface did not induce martensitic transformation, as there are only austenite peaks in Fig. 15. The thermal soften effect plays a primary impact at this cutting speed. The higher temperature reduces the dislocation density and stress, which leads to an inconsiderable peak broadening. Meanwhile, the increased cutting temperature reduces the dislocation and defect density [37], causing a more uniform microstructure on the surface. Under the cryogenic condition, it displays the highest peak, which can be concluded through quick cooling by LN₂, which causes a more uniform microstructure of the material.

4 Conclusions

The turning experiments of NiTi shape memory alloy at different cutting speeds under dry, flood, and LN₂ conditions were carried out in this work. It can be concluded that:

- When the cutting speed is less than 33 m/min, the mechanical effect is the dominant one for machinability. As the cutting speed increases, the thermal effect exceeds the mechanical effect and plays a primary role in turning.
- The stress-induced martensitic phase occurred during machining, which increased tool wear and surface roughness. But has little influence on the cutting force and machined samples' phase state.
- At a lower cutting speed (less than 33 m/min), flood conditions have a positive effect on the tool wear, cutting force, cutting temperature, and surface roughness, and a uniform microstructure is obtained, while, as the cutting speed increases, the flood condition has little influence on the machinability. At the cutting speed of 15 m/min, the machinability performs the best under flood conditions.
- The cryogenic condition reduces the cutting temperature effectively. When the cutting speed is more than 33 m/min, the lower cutting temperature decreases the tool wear, and quick cooling promotes the uniform microstructure. At 125 m/min, the best machining performance is displayed under cryogenic conditions according to the evaluation characteristic in this paper.

Authors' contribution Conceptualizations: Yanzhe Zhao and Jie Sun; methodology: Yanzhe Zhao, Jie Sun, and Kai Guo; investigation: Yanzhe Zhao and Jianfeng Li; writing, review, and editing: all the authors.

Funding This work was supported by the National Natural Science Foundation of China (51975335) and the Construction Engineering Special Fund of "Taishan Scholars" of Shandong Province (ts20190975).

Data Availability Not applicable.

Declarations

Ethics approval and consent to participate Not applicable

Consent to publish The copy permissions have been taken, and consent to submit has been received explicitly from all co-authors.

Conflict of interest The authors declare no competing interests.

References

1. Kowalczyk M (2018) Temperature distribution in the machining zone during precise turning of NiTi alloy. *Proc SPIE* 10808. <https://doi.org/10.1117/12.2501494>
2. Kowalczyk M (2017) Application of Taguchi method to optimization of surface roughness during precise turning of NiTi shape memory alloy. *Photonics Appl Astron Commun Ind High Energy Phys Exp* 2017 10445:104455G <https://doi.org/10.1117/12.2281062>
3. Bayati P, Safaei K, Nematollahi M, Ahmadreza J, Yadollahi A, Mahtabi M, Elahinia M (2021) Toward understanding the effect of remelting on the additively manufactured NiTi. *Int J Adv Manuf Technol* 112:347–360. <https://doi.org/10.1007/s00170-020-06378-4>
4. Lin HC, Lin KM, Chen YC (1999) The laser machining characteristics of TiNi shape memory alloys. *High Temp Mater Process* 3: 409–420
5. Kaya E, Kaya İ (2019) A review on machining of NiTi shape memory alloys: the process and post process perspective. *Int J Adv Manuf Technol* 100:2045–2087. <https://doi.org/10.1007/s00170-018-2818-8>
6. Debnath S, Reddy MM, Yi QS (2014) Environmental friendly cutting fluids and cooling techniques in machining: a review. *J Clean Prod* 83:33–47. <https://doi.org/10.1016/j.jclepro.2014.07.071>
7. Ezugwu EO (2005) Key improvements in the machining of difficult-to-cut aerospace superalloys. *Int J Mach Tools Manuf* 45:1353–1367
8. Kaynak Y, Karaca HE, Noebe RD, Jawahir IS (2013) Tool-wear analysis in cryogenic machining of NiTi shape memory alloys: a comparison of tool-wear performance with dry and MQL machining. *Wear* 306:51–63. <https://doi.org/10.1016/j.wear.2013.05.011>
9. Wu SK, Lin HC, Chen CC (1999) Study on the machinability of a Ti49.6Ni50.4 shape memory alloy. *Mater Lett* 40:27–32. [https://doi.org/10.1016/S0167-577X\(99\)00044-0](https://doi.org/10.1016/S0167-577X(99)00044-0)
10. Biermann D, Kahleiss F, Surmann T (2009) Micromilling of NiTi shape-memory alloys with ball nose cutters. *Mater Manuf Process* 24:1266–1273
11. Guo Y, Klink A, Fu C, Snyder J (2013) Machinability and surface integrity of Nitinol shape memory alloy. *CIRP Ann Manuf Technol* 62:83–86. <https://doi.org/10.1016/j.cirp.2013.03.004>
12. Weinert K, Petzoldt V, Kötter D (2004) Turning and drilling of NiTi shape memory alloys. *CIRP Ann - Manuf Technol* 53:65–68. [https://doi.org/10.1016/S0007-8506\(07\)60646-5](https://doi.org/10.1016/S0007-8506(07)60646-5)
13. Kuppaswamy R, Yui A (2017) High-speed micromachining characteristics for the NiTi shape memory alloys. *Int J Adv Manuf Technol* 93:11–21. <https://doi.org/10.1007/s00170-015-7598-9>

14. Biermann D, Kahleiss F, Krebs E, Upmeyer T (2011) A study on micro-machining technology for the machining of NiTi: five-axis micro-milling and micro deep-hole drilling. *J Mater Eng Perform* 20:745–751. <https://doi.org/10.1007/s11665-010-9796-9>
15. Wang G, Liu Z, Ai X, Huang W, Niu J (2018) Effect of cutting parameters on strain hardening of nickel-titanium shape memory alloy. *Smart Mater Struct* 27:075027. <https://doi.org/10.1088/1361-665X/aac43d>
16. Weinert K, Petzoldt V (2004) Machining of NiTi based shape memory alloys. *Mater Sci Eng A* 378:180–184. <https://doi.org/10.1016/j.msea.2003.10.344>
17. Kaynak Y, Robertson SW, Karaca HE, Jawahir IS (2015) Progressive tool-wear in machining of room-temperature austenitic NiTi alloys: the influence of cooling/lubricating, melting, and heat treatment conditions. *J Mater Process Technol* 215:95–104. <https://doi.org/10.1016/j.jmatprotec.2014.07.015>
18. Zailani ZA, Mativenga PT (2016) Effects of chilled air on machinability of NiTi shape memory alloy. *Procedia CIRP* 45:207–210. <https://doi.org/10.1016/j.procir.2016.02.156>
19. Rosnan R, Murad MN, Azmi AI, Shyha I (2019) Effects of minimal quantity lubricants reinforced with nano-particles on the performance of carbide drills for drilling nickel-titanium alloys. *Tribol Int* 136:58–66. <https://doi.org/10.1016/j.triboint.2019.03.029>
20. Mehrpouya M, Shahedin AM, Daood Salman Dawood S, Kamal Ariffin A (2017) An investigation on the optimum machinability of NiTi based shape memory alloy. *Mater Manuf Process* 32:1497–1504. <https://doi.org/10.1080/10426914.2017.1279290>
21. Yang H, Sakai K, Shizuka H, Kurebayashi Y, Hayakawa K (2021) Nagare T (2021) Experimental investigation of the effects of super-elasticity on the machinability of NiTi alloys. *Int J Adv Manuf Technol* 115:581–593. <https://doi.org/10.1007/s00170-021-07166-4>
22. Mohd Khalil AN, Azmi AI, Murad MN, Mahboob Ali MA (2018) The effect of cutting parameters on cutting force and tool wear in machining nickel titanium shape memory alloy ASTM F2063 under minimum quantity nanolubricant. *Procedia CIRP* 77:227–230. <https://doi.org/10.1016/j.procir.2018.09.002>
23. Kaynak Y (2014) Machining and phase transformation response of room-temperature austenitic NiTi shape memory alloy. *J Mater Eng Perform* 23:3354–3360. <https://doi.org/10.1007/s11665-014-1058-9>
24. A.R.C. S, J.I. H, K. R (2006) An analysis of the residual stresses generated in Inconel 718™ when turning. *J Mater Process Technol* 173:359–367
25. Pereira WH, Delijaicov S (2019) Surface integrity of INCONEL 718 turned under cryogenic conditions at high cutting speeds. *Int J Adv Manuf Technol* 104:2163–2177
26. Pusavec F, Deshpande A, Shu Y, M'Saoubi R, Jawahir IS (2015) Sustainable machining of high temperature Nickel alloy - Inconel 718: part 2 - chip breakability and optimization. *J Clean Prod* 87: 941–952
27. Madariaga A, Esnaola JA, Fernandez E, Arrazola PJ, Garay A, Morel F (2014) Analysis of residual stress and work-hardened profiles on Inconel 718 when face turning with large-nose radius tools. *Int J Adv Manuf Technol* 71:1587–1598
28. Kaynak Y, Karaca HE, Noebe RD, Jawahir IS (2015) The effect of active phase of the work material on machining performance of a NiTi shape memory alloy. *Metall Mater Trans A Phys Metall Mater Sci* 46:2625–2636. <https://doi.org/10.1007/s11661-015-2828-1>
29. Chaabani S, Arrazola PJ, Ayed Y, Madariaga A, Tidu A, Germain G (2020) Comparison between cryogenic coolants effect on tool wear and surface integrity in finishing turning of Inconel 718. *J Mater Process Technol* 285:116780. <https://doi.org/10.1016/j.jmatprotec.2020.116780>
30. Sivaiah P, Chakradhar D (2017) Influence of cryogenic coolant on turning performance characteristics: a comparison with wet machining. *Mater Manuf Process* 32:1475–1485
31. Benafan O, Noebe RD, Padula SA, Gaydos DJ, Lerch BA, Garg A, Bigelow GS, An K, Vaidyanathan R (2013) Temperature-dependent behavior of a polycrystalline NiTi shape memory alloy around the transformation regime. *Scr Mater* 68:571–574. <https://doi.org/10.1016/j.scriptamat.2012.11.042>
32. Benafan O, Noebe RD, Padula SA, Garg A, Clausen B, Vogel S, Vaidyanathan R (2013) Temperature dependent deformation of the B2 austenite phase of a NiTi shape memory alloy. *Int J Plast* 51: 103–121. <https://doi.org/10.1016/j.ijplas.2013.06.003>
33. Sivalingam V, Sun J, Yang B, Liu K, Ramesh RC (2018) Machining performance and tool wear analysis on cryogenic treated insert during end milling of Ti-6Al-4V alloy. *J Manuf Process* 36:188–196. <https://doi.org/10.1016/j.jmapro.2018.10.010>
34. Zhao Y, Li J, Guo K, Sivalingam V, Sun J (2020) Study on chip formation characteristics in turning NiTi shape memory alloys. *J Manuf Process* 58:787–795. <https://doi.org/10.1016/j.jmapro.2020.08.072>
35. Zhao YZ, Guo K, Sivalingam V, Li JF, Sun QD, Zhu ZJ, Sun J (2021) Surface integrity evolution of machined NiTi shape memory alloys after turning process. *Adv Manuf.* <https://doi.org/10.1007/s40436-020-00330-1>
36. Thakur A, Gangopadhyay S (2016) State-of-the-art in surface integrity in machining of nickel-based super alloys. *Int J Mach Tools Manuf* 100:25–54. <https://doi.org/10.1016/j.ijmactools.2015.10.001>
37. Kaynak Y, Huang B, Karaca HE, Jawahir IS (2017) Surface characteristics of machined NiTi shape memory alloy: the effects of cryogenic cooling and preheating conditions. *J Mater Eng Perform* 26:3597–3606. <https://doi.org/10.1007/s11665-017-2791-7>

Publisher's note Springer Nature remains neutral with regard to jurisdictional claims in published maps and institutional affiliations.